Nonlinear Vibration Analysis of FIAT Brava Chassis with 3-Cylinder DI Diesel Engine by Elastic Multibody Simulation

Dr. Peter **Fischer**, Wolfgang **Witteveen,** Robert **Premstaller**
Technologie Zentrum Steyr, Steyr Daimler Puch, Steyr

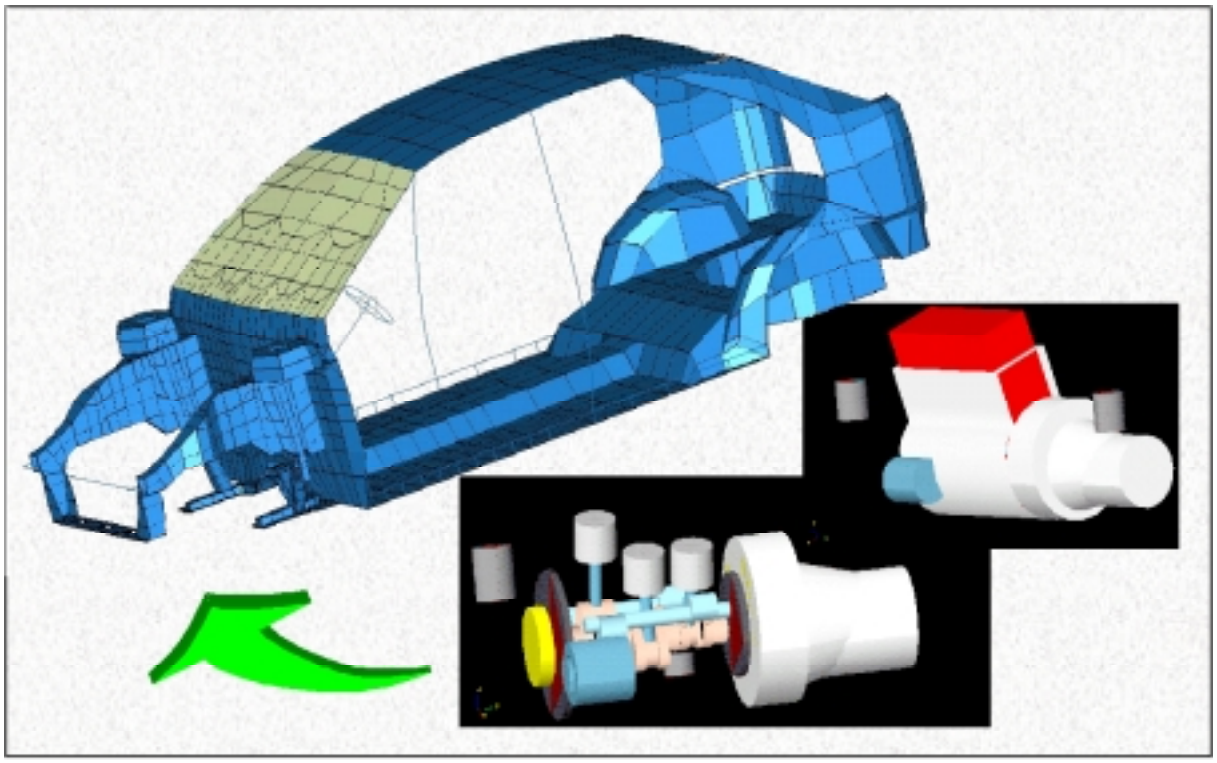

Figure 1: MBS and FE model of engine and chassis.

Abstract

Vibration comfort and interior noise of a vehicle chassis are critical design features. Depending on travelling and engine speed, the engine is an important source of excitation. The vibrations are transmitted by engine mounts to the vehicle body. Especially at low frequencies, like idle speed, the engine can be represented as an assembly of rigid bodies. The chassis, however, has to be treated as an elastic structure. Component mode synthesis will be used to combine the Multi Body System (MBS) of the engine with the Finite Element structure of the vehicle chassis.

First, the Multi Body System of the engine is modeled. This contains the engine block, the gearbox and all important movable parts. Besides the inertia effects, the excitation by combustion forces has to be taken into consideration. The engine assembly is suspended by engine mounts. The Finite Element model of the chassis may be coarse as it has to represent just those modes, which yield significant

response contributions at desired locations. The FE and MBS models are combined to a hybrid system by utilizing specific sets of FE modes which are imported and assembled by the MBS software. Vibrations at comfort locations of the chassis and engine mount forces are computed.

The comparison between computed and measured results shows good agreements. With the combination of theoretical analysis and measurements, noise and vibrations of the engine-chassis assembly were successfully reduced. Finally, for the vehicle with the 3-cylinder DI diesel engine a better noise level was obtained than for the original 4 cylinder engine.

1 INTRODUCTION

In automotive industry, vibration simulations are increasingly applied. The investigations focus mainly on isolated application of Multi Body Simulation [1] [2], FE analysis [3] or approximate analytical techniques [4] [5].

Here, a hybrid technique of Finite Element (FE) and Multi Body Simulation (MBS) is applied for fitting the STEYR M13 diesel engine into the FIAT BRAVA chassis. In the low frequency range and at low engine speeds, the body of the car is mainly excited by engine vibrations, which are transmitted into the elastic chassis by nonlinear engine mounts. In lightweight car bodies exists a strong interaction between engine, engine mounts and the chassis. An isolated investigation of the system "engine on mounts" and an isolated analysis of the system "chassis" provides valuable information about basic properties, however, can never reflect the dynamic properties of the compound system.

2 METHOD OF ANALYSIS

A systematic approach is applied, where in the first step, engine and chassis are treated as isolated structures. Since the frequency range of interest is relatively low (up to approximately 100 Hz), the engine is modeled as Multi Body Structure of rigid components. It includes the most important moveable parts (crankdrive, balance shafts) and the driving mechanism by the combustion forces. The engine is fixed to rigid ground by engine mounts. Basic investigations of engine modes, stiffness of engine mounts and support forces are performed.

The chassis can, by no means, be treated as a rigid body system in this frequency range. Typically, the lowest torsion and bending modes of the chassis are lower than 100 Hz. There are also frequently local effects like steering wheel modes and vibrations of the engine suspension girders. The chassis is modeled as a coarse FE structure. There is no need to include structural details. The FE model has just the task to represent the correct stiffness and the basic modes of interest. The chassis is tuned to the lowest torsion, bending and steering wheel modes of the vehicle. Modal analysis and computation of transfer functions are performed to assess the basic dynamic properties of the chassis.

As a final step, the coupled system "engine – engine mounts - chassis" is analyzed. This is performed by component mode synthesis of the FE and the MB structure. The shifts of eigenfrequencies and modeshapes of the coupled system compared to the isolated structures indicate the high degree of interaction. Response analysis for a series of engine speeds is performed in time domain. Frequency transforms and waterfall diagrams of the response are created for vibrations at comfort points [6] and of the forces transmitted by the engine mounts.

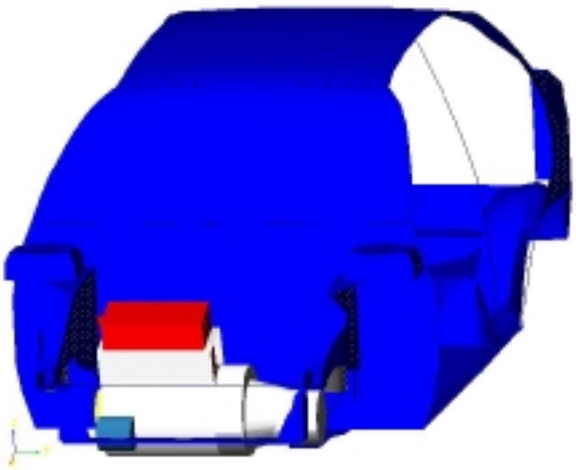

Figure 2: Coupled FE-MBS system.

3 THEORY

In order to perform the coupled analysis, the elastic properties of the chassis are imported into the MBS software package.

Figure 3: Hybrid analysis by import of FE Structures into MBS.

The representation of the flexible body requires the introduction of so called ‘modal coordinates’. This chapter contains a brief overview of the underlying theory.

3.1 Representation of the Flexible Body by Modal Coordinates

The representation of the flexible body isrealized by the introduction of so called ‘modal coordinates’. Figure 4 shows a general body undergoing an elastic deformation.

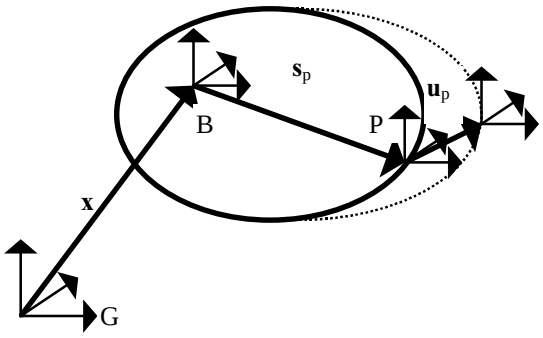

Figure 4: The position vector of a point P on a flexible body relative to a local reference frame B and ground G.

The position vector of point P on the flexible body, is defined as

$$\mathbf{r}_p = \mathbf{x} + \mathbf{s}_p + \mathbf{u}_p \quad . \tag{1}$$

x position vector from the origin ground reference frame to the origin of the local body reference frame, B, of the flexible body.

$\mathbf{s}_p$ position vector of the undeformed position of point P with respect to the ground reference frame, G.

$\mathbf{u}_p$ elastic displacement vector of point P. The vector is oriented from the point's undeformed position to its deformed position, with respect to the ground reference frame, G.

With respect to the ground reference frame the position vector $\mathbf{r}_p$ is written in matrix form as

$$\mathbf{r}_p = \mathbf{x} + {}^G\mathbf{A}^B \cdot (\mathbf{s}_P^B + \mathbf{u}_P^B) \quad . \tag{2}$$

${}^G\mathbf{A}^B$ transformation matrix from the local reference frame B to ground. Henceforth ${}^G\mathbf{A}^B$ is written as **A**.

$\mathbf{s}_P^B$ position vector of the undeformed position of point P with respect to local body reference frame, B.

$\mathbf{u}_P^B$ elastic displacement vector of point P with respect to the local body reference frame, B. The displacement of point P is approximated by linear combinations of shape functions:

$$\mathbf{u}_P^B \cong \sum_{k=1}^{M} \boldsymbol{\varphi}_{k(P)} \cdot q_k = \boldsymbol{\Phi}_{(P)} \cdot \mathbf{q}, \tag{3}$$

where

$\boldsymbol{\varphi}_{k(P)}$ is the k-th shape function evaluated at point P and

q_k is the corresponding time dependent modal coordinate.

By using Equation (3) equation (2) is written as

$$\mathbf{r}_p = \mathbf{x} + \mathbf{A} \cdot (\mathbf{s}_P^B + \boldsymbol{\Phi}_{(P)} \cdot \mathbf{q}). \tag{4}$$

In the following the vector $\boldsymbol{\xi}$ of generalized coordinates of the flexible body is introduced.

$$\boldsymbol{\xi} = \begin{Bmatrix} x \\ y \\ z \\ \psi \\ \theta \\ \phi \\ q_{i,i=1..n} \end{Bmatrix} \tag{5}$$

The components x, y, z, ψ, θ and ϕ denote the translational and rotational displacements of the undeformed body.

This vector of generalized coordinates is used for the Lagrange's equation [A].

$$\begin{aligned} &\frac{d}{dt}\left(\frac{\partial L}{\partial \dot{\boldsymbol{\xi}}}\right) - \frac{\partial L}{\partial \boldsymbol{\xi}} + \left[\frac{\partial \boldsymbol{\Psi}}{\partial \boldsymbol{\xi}}\right]^T \cdot \boldsymbol{\lambda} - \mathbf{Q} = 0 \\ &\boldsymbol{\Psi} = 0 \end{aligned} \tag{6}$$

L Lagrangian, defined as L = T-V.

T kinetic energy.

V potential energy.

$\boldsymbol{\Psi}$ vector of the constraint equations.

$\boldsymbol{\lambda}$ vector of the Lagrange multipliers for the constraints.

$\mathbf{Q}$ vector of the generalized forces, due to externally applied forces.

$\boldsymbol{\xi}$ generalized coordinates as defined in equation (5).

Section 3.3 gives a brief idea how the MBS software solves the Lagrange's equation of motion.

3.2 Determination of Modal Coordinates - Importing FE Model into MBS

As mentioned above, a set of shape functions, generally a set of eigenvectors is used to approximate the deformation of an elastic body. These shape functions should have following characteristics:

- The set of eigenvectors should not depend on the boundary conditions in the MBS.
- The number of degrees of freedom in the MBS should not increase dramatically.
- These are the main features of a family of techniques called 'component mode synthesis', which is applied by ADAMS.

3.2.1 General Equation of Motion

A component with the stiffness matrix **K** and the lumped mass matrix **M** is considered. By neglecting the damping, the equation of motion is

$$\mathbf{M} \cdot \ddot{\boldsymbol{\delta}} + \mathbf{K} \cdot \boldsymbol{\delta} = \mathbf{f} \,. \tag{7}$$

M lumped mass matrix of a component (e.g. of a FE - structure, n x n matrix)

K stiffness matrix of this component (n x n) matrix

δ vector of displacements. (n x 1)

f load vector (n x 1)

Note the disadvantages:

- It's a coupled system
- Considering a complex model (for example a FE model of an engine frame) leads to a high number of degrees of freedom n, e.g. 500000.

3.2.2 Applying the Theory of Craig Bampton [9].

A structure with a number of interface points is considered. Interface points are those points at which constraints or external forces may be applied. The elastic deformation of this structure can be described by superposition of the so called 'interface constraint modes' and the 'interface normal modes'.

Constraint modes are the static shapes of the component when one degree of freedom at one interface point undergoes a unit deflection while keeping all other degrees of freedom fixed.

Interface normal modes are the eigenvectors of the component with all interface degrees of freedom fixed.

The degrees of freedom of system (7) can be split into two parts. The degrees of freedom of the interface or boundary points, $\boldsymbol{\delta}^B$, and the interior points, $\boldsymbol{\delta}^I$. $\boldsymbol{\delta}^I$ and $\boldsymbol{\delta}^B$ denote physical displacements.

$$\begin{bmatrix} \mathbf{M}^{BB} & 0 \\ 0 & \mathbf{M}^{II} \end{bmatrix} \cdot \begin{bmatrix} \ddot{\boldsymbol{\delta}}^B \\ \ddot{\boldsymbol{\delta}}^I \end{bmatrix} + \begin{bmatrix} \mathbf{K}^{BB} & \mathbf{K}^{BI} \\ \mathbf{K}^{IB} & \mathbf{K}^{II} \end{bmatrix} \cdot \begin{bmatrix} \boldsymbol{\delta}^B \\ \boldsymbol{\delta}^I \end{bmatrix} = \begin{bmatrix} \mathbf{f}^B \\ \mathbf{f}^I \end{bmatrix} . \tag{8}$$

Considering the static case the resulting force at an interior point and the inertia effects vanish and the second line of system (8) can be written as

$$\mathbf{K}^{IB} \cdot \boldsymbol{\delta}^B + \mathbf{K}^{II} \cdot \boldsymbol{\delta}^I = 0 . \tag{9}$$

Rearranging equation (9) and introducing $\hat{\boldsymbol{\Phi}}^C = -(\mathbf{K}^{II})^{-1} \cdot \mathbf{K}^{IB}$ leads to

$$\boldsymbol{\delta}^I = -(\mathbf{K}^{II})^{-1} \cdot \mathbf{K}^{IB} \cdot \boldsymbol{\delta}^B = \hat{\boldsymbol{\Phi}}^C \cdot \boldsymbol{\delta}^B . \tag{10}$$

It is seen that a row of the matrix $\hat{\boldsymbol{\Phi}}^C$ contains the static deformation of $\boldsymbol{\delta}^I$ due to an unit deflection of the associated interface point. $\hat{\boldsymbol{\Phi}}^C$ is the matrix of constraint modes.

Additionally to the constraint modes the normal modes of the component with all boundary degrees of freedom fixed are obtained by solving the appropriate eigenvalue problem. The eigenvalue problem leads to a matrix of normal modes $\boldsymbol{\Phi}^N$. Theoretically, there are so many modes (rows in the matrix) as degrees of freedom. However, generally a set of truncated modes $\hat{\boldsymbol{\Phi}}^N$ is used.

The main idea of the Craig Bampton Method is to approximate the physical coordinates $\boldsymbol{\delta}^I$ and $\boldsymbol{\delta}^B$ by a summation of constraint and normal modes:

$$\begin{bmatrix} \boldsymbol{\delta}^B \\ \boldsymbol{\delta}^I \end{bmatrix} = \begin{bmatrix} \mathbf{I} & \mathbf{0} \\ \hat{\boldsymbol{\Phi}}^C & \hat{\boldsymbol{\Phi}}^N \end{bmatrix} \cdot \begin{bmatrix} \mathbf{q}^C \\ \mathbf{q}^N \end{bmatrix} = \hat{\boldsymbol{\Phi}} \cdot \mathbf{q} , \tag{11}$$

where **q** are modal coordinates.

Note the second line of the equation:

$$\boldsymbol{\delta}^I = \hat{\boldsymbol{\Phi}}^C \cdot \mathbf{q}^C + \hat{\boldsymbol{\Phi}}^N \cdot \mathbf{q}^C \tag{12}$$

The displacement of interior nodes is approximated as a superposition of the vibrations from the structure fixed at the interface points and the static mode shapes due to the displacement of the interface points.

Using (11) equation (7) can be approximated by

$$\hat{\boldsymbol{\Phi}}^T \cdot \mathbf{M} \cdot \hat{\boldsymbol{\Phi}} \cdot \ddot{\mathbf{q}} + \hat{\boldsymbol{\Phi}}^T \cdot \mathbf{K} \cdot \hat{\boldsymbol{\Phi}} \cdot \mathbf{q} = \hat{\boldsymbol{\Phi}}^T \cdot \mathbf{f} = \hat{\mathbf{M}} \cdot \ddot{\mathbf{q}} + \hat{\mathbf{K}} \cdot \mathbf{q} = \mathbf{g} . \tag{13}$$

q = vector of modal coordinates (1 x m).

$\mathbf{g} = \hat{\mathbf{\Phi}}^T \cdot \mathbf{f} = \begin{Bmatrix} \mathbf{f}_B \\ 0 \end{Bmatrix}$. Dimension of **g**: 1 x m.

$\hat{\mathbf{M}} = \hat{\mathbf{\Phi}}^T \cdot \mathbf{M} \cdot \hat{\mathbf{\Phi}}$

$\hat{\mathbf{K}} = \hat{\mathbf{\Phi}}^T \cdot \mathbf{K} \cdot \hat{\mathbf{\Phi}}$.

Note the advantages:

- The set of shapes and modes are independent of the boundary conditions in the MBS.
- m is the number of the interface normal modes plus the sum of all degrees of freedom of the interface points. m is significant smaller than n.
- Analyzing $\hat{\mathbf{M}}$, $\hat{\mathbf{K}}$ and **g** shows that this system is only partially coupled.

Note the disadvantages:

- The system is not fully decoupled
- A large number of interface points, results in a large number of constraint modes. It is difficult to decide, which constraint modes are important and which can be neglected.
- The constraint modes can introduce high frequency contents into the system.

3.2.3 Constraint Mode Orthogonalization

Equation (13) leads to the eigenvalue problem (14):

$$\hat{\mathbf{K}} \cdot \mathbf{r} = \sigma \cdot \hat{\mathbf{M}} \cdot \mathbf{r} \qquad (14)$$

After solving the eigenvalue problem (14) the eigenvectors **r** are collected into the matrix **R** and the appropriate eigenvalues σ into the diagonal matrix $\mathbf{\Sigma}$.

The normal modes and the constraint modes described in the previous section are converted into new modes. Visualizing this modified mode shapes shows that they consist of two families of shapes.

The normal modes of the unconstrained component.

Mode shapes that one could refer to as interface eigenvectors because they constitute the solution of the eigenvalue problem for the interface degrees of freedom.

Substituting **R** into (13) leads to

$$\begin{aligned} &\mathbf{R}^T \cdot \hat{\mathbf{M}} \cdot \mathbf{R} \cdot \ddot{\overline{\mathbf{q}}} + \mathbf{R}^T \cdot \hat{\mathbf{K}} \cdot \mathbf{R} \cdot \overline{\mathbf{q}} = \mathbf{R}^T \cdot \mathbf{g} = \\ &\mathbf{I} \cdot \ddot{\overline{\mathbf{q}}} + \mathbf{\Sigma}^2 \cdot \overline{\mathbf{q}} = \mathbf{b} \end{aligned} \quad . \tag{15}$$

$\mathbf{I}$ identity matrix (m x m). $\mathbf{I} = \mathbf{R}^T \cdot \hat{\mathbf{M}} \cdot \mathbf{R}$

$\mathbf{\Sigma}$ diagonal matrix of the eigenvalues of the eigenvalue problem (14).

$\mathbf{\Sigma}^2 = \mathbf{R}^\mathbf{T} \cdot \hat{\mathbf{K}} \cdot \mathbf{R}$

$\mathbf{b}$ transformed load vector.

$\mathbf{b} = \mathbf{R}^T \cdot \mathbf{g}$

Note the advantages:

- The system is fully decoupled.
- All advantages of the Craig Bampton transformation (section 3.2.2) are valid.
- Each mode is associated with an eigenfrequency.

3.2.4 Summary

A FE program computes the interface normal modes with fixed interface points. Furthermore the FE program computes the shapes of the component when one degree of freedom at one interface point undergoes a unit deflection while holding all other degrees of freedom fixed. After transferring all these modes and shapes into the MBS software, a new set of modes will be created by means of the component mode synthesis. The number of these modes determines the additional degrees of freedom. Each mode introduces a modal coordinate to the Lagrange's equation (refer to section 3.1).

3.3 Numerical Solution of the Elastic Multi Body System

Utilizing the modal coordinates $\overline{\mathbf{q}}$, the Lagrange's equation (6) is solved similar as a standard non-flexible problem. System (6) is written as

$$\begin{Bmatrix} \mathbf{F} \\ \mathbf{\Psi} \end{Bmatrix} = \{\mathbf{0}\}. \tag{16}$$

where

$$\mathbf{F} = f(\ddot{\boldsymbol{\xi}}, \dot{\boldsymbol{\xi}}, \boldsymbol{\xi}, \boldsymbol{\lambda}, t)\ ,\ \boldsymbol{\xi} = [\xi_1, \xi_2, ...\xi_n]^T \text{ and } \boldsymbol{\lambda} = [\lambda_1, \lambda_2, ...\lambda_m].$$

After reducing the terms of second order by introducing $\mathbf{u} = \frac{d\boldsymbol{\xi}}{dt}$, equation (16) is rearranged as

$$\begin{Bmatrix} \mathbf{F} \\ \dot{\boldsymbol{\xi}} - \mathbf{u} \\ \boldsymbol{\psi} \end{Bmatrix} = \{\mathbf{0}\}, \tag{17}$$

where

$$\mathbf{F} = f(\dot{\mathbf{u}}, \mathbf{u}, \dot{\boldsymbol{\xi}}, \boldsymbol{\xi}, \boldsymbol{\lambda}, t)\,.$$

This operation reduces the second order differential equations to a first order differential equation. However, the number of degrees of freedom increases.

The solution of system (17) provides all forces, velocities, displacements and accelerations. This equation can only be solved by a numerical algorithm. The MBS software ADAMS utilizes a Gear predictor-corrector [D] algorithm. The algorithm performs a prediction and a correction step in order to compute the solution.

Based on the Taylor series

$$\mathbf{y}_{s+1} = \mathbf{y}_s + \frac{\partial \mathbf{y}_s}{\partial t} h + \frac{1}{2} \frac{\partial^2 \mathbf{y}_s}{\partial t^2} h^2 + \ldots\ldots \quad , \tag{18}$$

where $h = t_{s+1} - t_s$ (integration time step), the system state for the next time step is predicted. The vector **y** is in general a vector of the degrees of freedom and represents the system state.

The general form of one of the correctors used in ADAMS, the Gear stiff integrator of order k+1, is

$$\mathbf{y}_{s+1} = -h \cdot \beta_0 \cdot \dot{\mathbf{y}}_{s+1} + \sum_{j=1}^{k} a_j \mathbf{y}_{s-j+1}\,. \tag{19}$$

The parameters β_0, a_i are gear integration coefficients. Equation (19) can be rearranged to

$$\dot{\mathbf{y}}_{s+1} = \frac{-1}{h \cdot \beta_0} \left(\mathbf{y}_{s+1} - \sum_{j=1}^{k} a_j \cdot \mathbf{y}_{s-j+1} \right). \tag{20}$$

The task of the corrector is to adjust the systems variables such, that the solution of equation (17) is within a tolerable error margin.

When $\mathbf{p} = \dot{\boldsymbol{\xi}} - \mathbf{u}$ is introduced and using equation (20), equation (17) can be written for time instant s+1 as

$$\mathbf{F}\left(\dot{\mathbf{u}}_{s+1}, \mathbf{u}_{s+1}, \boldsymbol{\xi}_{s+1}, \boldsymbol{\lambda}_{s+1}, t_{s+1}\right) = \mathbf{0} \tag{21}$$

$$\mathbf{p}(\mathbf{u}_{s+1},\boldsymbol{\xi}_{s+1}) = \dot{\boldsymbol{\xi}}_{s+1} - \mathbf{u}_{s+1} = \left(\frac{-1}{h\beta_0}\right)\left(\boldsymbol{\xi}_{s+1} - \sum_{j=1}^{k} a_j \cdot \boldsymbol{\xi}_{s-j+1}\right) - \mathbf{u}_{s+1} = \mathbf{0} \tag{22}$$

$$\boldsymbol{\Psi}(\boldsymbol{\xi}_{s+1}, t_{s+1}) = \mathbf{0}\,. \tag{23}$$

If the time is fixed and the equations (21), (22) and (23) are expanded around their predicted values, the following set of equations is obtained [D]

$$\mathbf{F}_{s+1} + \frac{\partial \mathbf{F}}{\partial \boldsymbol{\xi}}\Delta\boldsymbol{\xi}_{s+1} + \frac{\partial \mathbf{F}}{\partial \mathbf{u}}\Delta\mathbf{u}_{s+1} + \frac{\partial \mathbf{F}}{\partial \dot{\mathbf{u}}}\Delta\dot{\mathbf{u}}_{s+1} + \frac{\partial \mathbf{F}}{\partial \boldsymbol{\lambda}}\Delta\boldsymbol{\lambda}_{s+1} = \mathbf{0}\,, \tag{24}$$

$$\mathbf{p}_{s+1} + \frac{\partial \mathbf{p}}{\partial \boldsymbol{\xi}}\Delta\boldsymbol{\xi}_{s+1} + \frac{\partial \mathbf{p}}{\partial \mathbf{u}}\Delta\mathbf{u}_{s+1} = \mathbf{0} \qquad \text{and} \tag{25}$$

$$\boldsymbol{\Psi}_{s+1} + \frac{\partial \boldsymbol{\Psi}}{\partial \boldsymbol{\xi}}\Delta\boldsymbol{\xi}_{s+1} = \mathbf{0}\,. \tag{26}$$

The change in $\dot{\mathbf{u}}$ may be related to the change in $\mathbf{u}$ by the relationship shown in (20) as

$$\Delta\dot{\mathbf{u}}_{s+1} = -\left(\frac{-1}{h\cdot\beta_o}\right)\Delta\mathbf{u}_{s+1}\ . \tag{27}$$

Comparing equation (25) to equation (22) shows that

$$\frac{\partial \mathbf{p}}{\partial \boldsymbol{\xi}} = \left(\frac{-1}{h\cdot\beta_0}\right)\cdot\mathbf{I} \qquad \text{and} \tag{28}$$

$$\frac{\partial \mathbf{p}}{\partial \mathbf{u}} = -\mathbf{I}. \tag{29}$$

By substituting equations (27)-(29) into equations (24)-(26), the result for a time instant s+1 is

$$\begin{bmatrix} \dfrac{\partial \mathbf{F}}{\partial \boldsymbol{\xi}} & \dfrac{\partial \mathbf{F}}{\partial \mathbf{u}} - \dfrac{1}{h\cdot\beta_0}\dfrac{\partial \mathbf{F}}{\partial \dot{\mathbf{u}}} & \left(\dfrac{\partial \boldsymbol{\Psi}}{\partial \boldsymbol{\xi}}\right)^T \\ \dfrac{-1}{h\cdot\beta_0}\cdot\mathbf{I} & -\mathbf{I} & \mathbf{0} \\ \left(\dfrac{\partial \boldsymbol{\Psi}}{\partial \boldsymbol{\xi}}\right) & \mathbf{0} & \mathbf{0} \end{bmatrix} \begin{Bmatrix} \Delta\boldsymbol{\xi}_{s+1} \\ \Delta\mathbf{u}_{s+1} \\ \Delta\boldsymbol{\lambda}_{s+1} \end{Bmatrix} = -\begin{Bmatrix} \mathbf{F}_{s+1} \\ \dot{\boldsymbol{\xi}}_{s+1} - \mathbf{u}_{s+1} \\ \boldsymbol{\Psi}_{s+1} \end{Bmatrix}. \tag{30}$$

This equation is solved iteratively for $\Delta\boldsymbol{\xi}_{s+1}, \Delta\mathbf{u}_{s+1}$ and $\Delta\boldsymbol{\lambda}_{s+1}$ of each time step by a suitable algorithm. The matrix on the left side of equation (30) is the system Jacobian. To summarize, equation (18) predicts the new system state and Equation

(30) leads the system equations to convergence. Note, that the terms in the Jacobian matrix show some well known structural effects, namely

$\frac{\partial \mathbf{F}}{\partial \boldsymbol{\xi}}$ ..... stiffness,

$\frac{\partial \mathbf{F}}{\partial \mathbf{u}}$ ..... damping,

$\frac{\partial \mathbf{F}}{\partial \dot{\mathbf{u}}}$ ..... inertia effects.

4 ENGINE

4.1 Design of Steyr M13 Diesel Engine

The Steyr M13 is a 3 cylinder direct injection diesel engine. It has a special design for low noise emission. The engine can be characterized by three main parts (see also figure 1):

- The central part is the monoblock which consists of the cylinders and the cylinder head. It is manufactured from one piece. At the bottom of the monoblock, the main bearing frame and the bearing caps are fixed.

- The second part is the engine housing. It is a stiff cover around the monoblock. On the one hand it acts as oil pan and noise capsule, on the other hand it supports the monoblock and carries also the brackets for the engine mounts.

- The "ring carriers" are elements, which provide an elastic connection between monoblock and engine housing. They have to be weak enough to decouple the vibrations of the monoblock and the engine housing, but they also have to be stiff enough to transmit the engine torque and all other forces acting on the block.

This concept has good acoustic properties especially concerning higher frequencies. However, there exists a disadvantage in the low frequency range. Up to 100 Hz, so called "ring carrier modes" occur, see figure 7. The monoblock and the engine housing vibrate relative to each other (like rigid bodies) by distortion of the elastomer ring carriers. This is also the frequency range where strong interactions of "engine - engine mounts - elastic chassis" occur in combination with main excitation forces by the lowest engine orders. To make fully advantage of the M13 concept, these phenomena have to be carefully investigated and optimized.

4.2 Model for Multi Body Simulation

To asses the dynamic behavior of the engine, the inertia of the structural components and the excitation mechanisms have to be modeled carefully (see figure 1).

Crank Drive: The crank shaft is connected to the monoblock by a revolute joint. It carries discrete mass points which represent the weight and the mass balancing. The pistons are guided by translational joints in the monoblock. The mass of the connecting rod is realized by a classical two-point separation, where the rotating part is added to the crankshaft and the oscillating part to the piston mass.

Balance Shafts: A three cylinder engine typically has unbalanced mass moments of the first and second order. To balance the moment of the first order, the M13 engine has a balance shaft with two oppositely aligned excenter weights. The balance shaft of the MB model is fixed to the monoblock by a revolute joint. It rotates in the opposite direction of the crankshaft.

Ring Carriers: The elastomer properties of the ring carriers between monoblock and engine housing are represented by a local stiffness and damping model. Depending on the relative distortion and velocity, restoring and damping forces are generated. This model is basically nonlinear, however, there were only linear stiffness and damping data available.

Inertia and Masses: The masses were either given or determined by weighting. The moments of inertia of the monoblock and the engine housing were obtained from existing Finite Element models. The moment of inertia of the gear box was initially estimated and further on fine tuned by comparison of computed and measured eigenfrequencies.

Excitation by Gas Forces: The effect of gas forces may be split in two mechanisms: first, there is a vertical force (in-line with the cylinder axis) which is in equilibrium concerning forces and moments. The second mechanism is the piston side force (horizontal) which results from the inclination of the conrod. It is in equilibrium with respect to forces, but not with respect to moments. The reaction of the piston side force is transmitted by the crank drive and is supported horizontally by the main bearings. This means that for any engine a considerable pulsating rolling moment exists. The moment is transferred to the engine mounts and cannot be balanced by counterweights or balance shafts. It is also not affected by the size of the flywheel mass. In the MB model, the piston side force of each cylinder is defined as a spline function in dependence of time. The force moves up and down according to the piston position. The counter force is applied at the main bearings.

4.3 Nonlinear Engine Mounts

The engine mounts are elastomer components with nonlinear stiffness. The characteristics were determined by measurements in dependence of amplitude, preload and frequency. The stiffness of the engine mounts was introduced into the MB model by spline functions which determine the relation between force and displacement. The frequency dependence cannot be reproduced by such a model. As long as the range of investigated engine speeds is small enough (e.g. 1000 to

2000 rpm), the measurements showed a sufficiently small stiffness variation. This is also in agreement with other investigations, see e.g. reference [10].

The vibration amplitudes are orders of magnitudes smaller than the static deformations resulting from engine weight and torque. The nonlinearity is therefore governed by the (quasi)static preloads. In the vicinity of the operating point of the static deflection, an elastomer mount behaves essentially linear. One notes that the operating point of static deflection can be easily mistuned by alignment modifications or by assembly preloads.

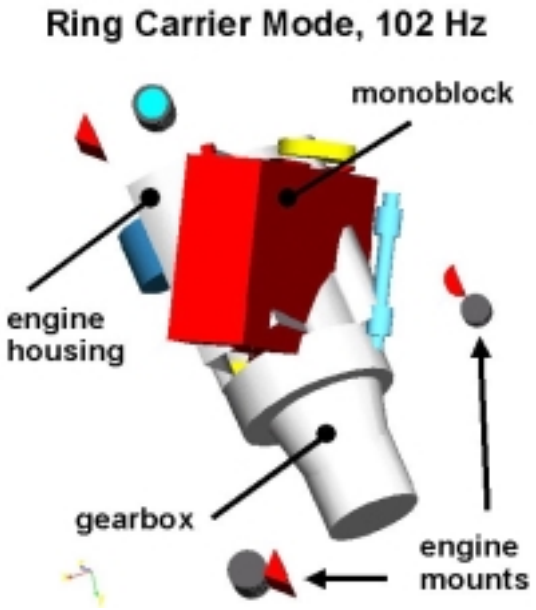

Figure 5: Example mode shape of engine fixed to ground.

4.4 Tuning of MBS Model

For primary investigations the MBS model was fixed to ground by means of the engine mounts. The dynamic properties of the model were tuned by comparison to measured eigenfrequencies and modeshapes. The tuning targets were the fundamental rigid body modes of pitching, rolling and yawing, which were clearly identified by measurements (see table 1). The tuning parameters were the rotational inertia values of the engine and the gravity centers and inertia values of the gearbox and the aggregates.

The modal analysis was performed by the MBS software. As the eigenvalue computation is based on linear structural matrices, the stiffness is linearized around the state of static deflection. Figure 5 shows an example mode at 102 Hz. The monoblock yawns in antiphase to the engine housing. This is an effect of the elastic ring carriers.

The modal analysis provides good ideas concerning the basic properties of the system. There exist e.g. predefined target frequency ranges for certain mode types

like pitching or rolling. Important influences, like engine mount positions or a different distribution of the stiffness among the mounts can be investigated.

4.5 Response Analysis, Engine Fixed to Ground

The response analysis is performed in time domain. It includes nonlinearities like engine mounts and spatial shifts of excitation forces as well as gyroscopic effects of rotating parts.

The analysis is divided into three sequences. In the first step the weight of the engine is applied to adjust the static equilibrium. In the second step, the crankshaft is accelerated linearly to the stationary speed level. The time dependency of the excitation forces is defined by the camshaft angle. Therefore the forces are automatically in phase with the engine revolutions. In the third step, the speed of the engine is kept constant. An approximately stationary state of the response was generally reached before 20 revolutions. The analysis was continued to 40 revolutions to obtain a sufficiently long period of stationary vibrations (see figure 6).

The solution turned out to be stable and fast, the computation time on a medium class workstation (SGI Octane) was about 10 minutes for 40 revolutions.

The analysis provides results for all displacements and forces which are specified. Results of main interest are the forces which are transmitted by the engine mounts. In particular, the frequency transform as e.g. depicted in figure 6 contains valuable information. It shows that the response is excitation dominated by several engine orders. The first order is well balanced and does almost not appear in the response. The major peak occurs at the 1.5-th order. It originates from the piston side forces of the 3 cylinder engine. There exists a small peak of the 2-nd order which results from the unbalanced mass moments. All higher peaks are multiples of the 1.5-th order. The basic eigenfrequencies of the engine don't interfere with the excitation frequencies.

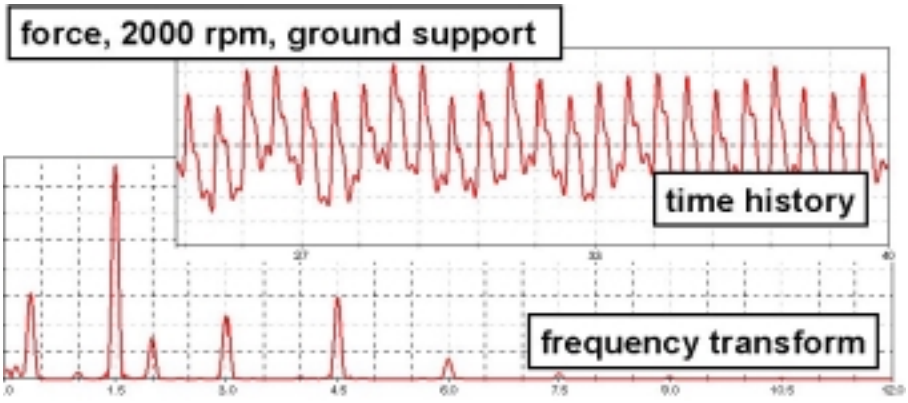

Figure 6: Forces in engine mount, 2000 rpm, supported by ground.

5 CHASSIS

5.1 FE Model of Chassis

The FE model has to represent the dynamic properties of interest, which are:

- the global stiffness of the chassis
- the stiffness of the vehicle front end and the engine girders
- the lowest global modes of the body
- some specific local modes of interest.

As long as the above specifications are justified, it is not required to include structural details. The model can be considered as a "phenomenological" structure which behaves the same way as the fully equipped vehicle at the spots and frequencies of interest.

Such a structure can be modeled in a rather coarse way. This is also an advantage concerning its practical use in the Multi Body Simulation. The structure was modeled exclusively by thin shell and beam elements having 6 degrees of freedom per node. This has the practical aspect of avoiding problems with free rotational DOF's of the FE model in the MB simulation. The model consists of 2200 shell and 600 beam elements. It has 2600 nodes and about 15000 DOF's. Increased attention was paid to a correct modeling of components like the front end girders, side rails and A-B-C columns.

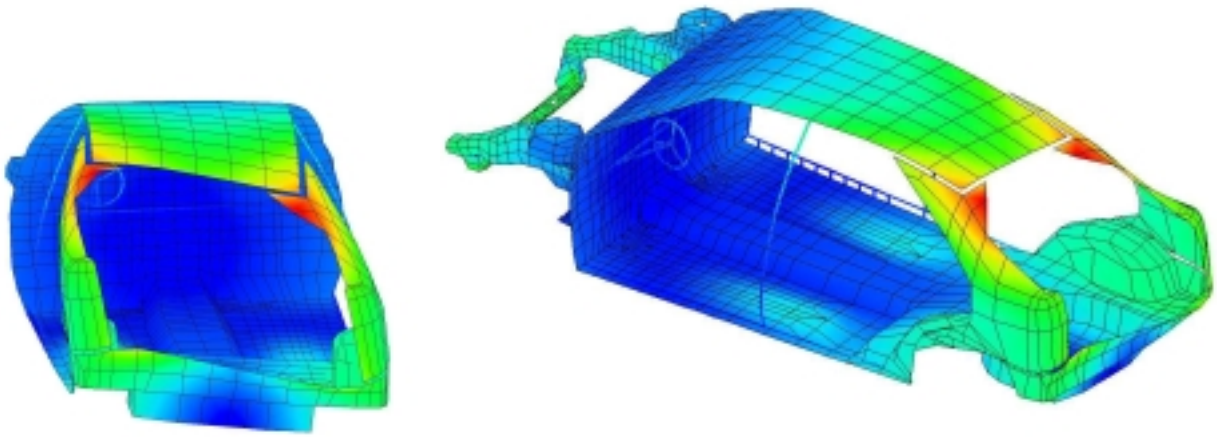

Figure 7: FE model and 1-st torsion mode shape of the chassis.

5.2 Tuning of FE Model

The FE model of the chassis was trimmed to the lowest torsion and bending mode of the fully equipped vehicle without the engine. Additionally, steering column and steering wheel were introduced and tuned, since the vehicle had unpleasant steering wheel vibrations which did not occur with the original engine. The computational modal analysis was performed with the FE solver. Figure 7 shows the principal torsion mode of the chassis at 43 Hz.

5.3 Response Analysis of Chassis Body

The real vehicle is a complex assembly of metallic parts, plastic components, composites, etc., which has considerable nonlinearities. However, the FE model represents a completley linear metallic structure. The response analysis of the FE model (without engine) was performed to highlight these effects and to compare the simulation results to measurements. Base of the comparison were transfer functions, which are the ratio between a single response and a single point excitation. Transfer functions are defined in the frequency domain, see e.g. reference [11].

In numerical simulation, transfer functions are obtained by exciting the structure with a sine of unit amplitude. When sweeping the excitation sine over the frequency range of interest, the corresponding amplitudes at a certain response location represent the transfer function.

The adjustment of modal damping values is one of the primary tasks when comparing computed and measured transfer functions. The peak of the computed response is inversely proportional to the modal damping value. Tuning the modal damping values means scaling of the response peaks.

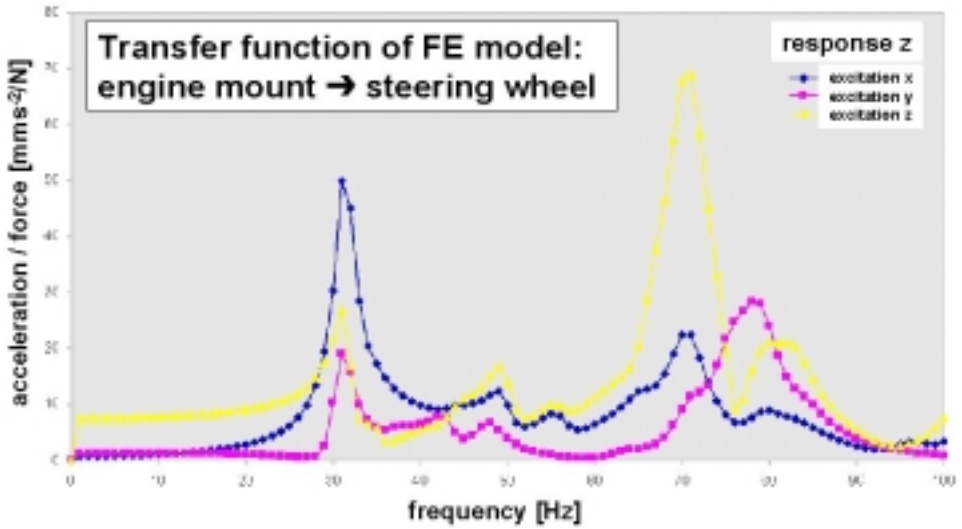

Figure 8: Transfer functions, engine girder - steering wheel, FE analysis.

The comparison of computed and measured transfer functions additionally provides an idea about the degree of nonlinearity of the real system. The computation is based on a linear system which generally shows a distinct peak-valley characteristic (see figure 8). In nonlinear reality the modepeaks change their shape, they frequently become wider at the base and more peaky at the top. The strongest differences between linear computation and nonlinear reality occur in the frequency ranges between the modepeaks. In these regions, the real response is up to several factors higher than the linear simulations.

Simulation: Engine supported by ground		Simulation: Engine supported in chassis		Measured: Engine in chassis	
eigenfreq. [Hz]	mode description	eigenfreq. [Hz]	mode description	eigenfreq. [Hz]	mode description
		3,13	vertical transl. of engine, pitching chassis		
4,54	axial translation of engine assembly	3,49	axial translation of engine, rolling chassis		
		4,53	combined rot./transl. of engine and chassis		
5,21	vertical translation of engine assembly			4,97	vertical translation of engine
5,38	lateral translation of engine assembly				
		7,39	combined rot./transl. of engine and chassis	8,11	combined rot./lateral transl. of engine
				9,42	combined rot./lateral transl. of engine
10,74	pitching of engine assembly	10,38	pitching of engine assembly	10,69	pitching of engine assembly
11,80	rolling engine assembly	10,76	rolling of engine assembly	11,93	rolling of engine assembly
12,59	yawing of engine assembly	12,00	yawing of engine assembly	14,01	yawing of engine assembly
		31,50	steering wheel vertical, front sheet		
		32,07	steering wheel vertical/horizontal		
42,69	axial deformation of ring carriers	42,95	axial deformation of ring carriers		
		46,20	torsion chassis, global		
		52,00	torsion chassis front frame		
66,63	torsion deformation ring carriers	66,53	torsion ring carrier, front fram		
97,77	front ring carrier, ajar vertical	95,07	front ring carrier, ajar vertical		
101,42	front ring carrier, ajar lateral	101,42	front ring carrier, ajar lateral		
128,15	rear ring carrier, ajar vertical	128,17	rear ring carrier, ajar vertical		
149,09	rear ring carrier, ajar lateral	142,33	rear ring carrier, ajar lateral		

Table 1: Comparison of eigenfrequencies, engine fixed to ground - engine in chassis.

6 COUPLED FE-MBS SYSTEM (HYBRID MODEL)

6.1 Coupling by Mode Synthesis

The coupling of the FE and MBS system is based on the principle of component mode synthesis, see e.g. [12]. The method is implemented into the MBS software ADAMS in form of a modified Craig-Bampton approach [13, 14].

In practice, two sets of displacement shapes of the finite element structure are required [15]. The first set consists of mode shapes, where the FE structure is fixed at the interface points to the MB structure. The second set (”constraint modes”) are static deflections, where each interface point undergoes a unit displacement. Both mode sets are created by the FE software NASTRAN. The computation is automated by a specific solution sequence (Nastran DMAP). The output is an ASCII file which contains the mode sets and additional information about the FE structure. This file is imported into the Multi Body Software, which assembles the total structure by applying component mode synthesis.

6.2 Modal Analysis of Coupled System

For the modal analysis of the hybrid system, the vehicle chassis was attached to ground by springs and dampers that approximately represent the suspension system and the tires.

The results of the eigenfrequency computations are summarized in table 1. It compares the computed eigenfrequencies of the engine – chassis assembly, the case when the engine is fixed to ground and the measured modes when the engine is mounted in the chassis.

Several different characteristics can be identified with respect to certain sets of modes. For the mode set of pitching, rolling and yawing occur only small differences between measurements and the two simulation cases (max. 9%).

The ring carrier modes of the engine (where the monoblock moves relative to the engine housing) are well separated from the fundamental chassis modes and the local steering wheel vibrations. Only minor frequency shifts occur when connecting engine and chassis.

However, a very high sensitivity is observed for the lowest translational modes of the engine. There is a completely different behavior when the engine is fixed to ground or when it is supported in the elastic chassis. The eigenfrequencies in the chassis differ up to 40%. The sequence of modes changes and new modeshapes occur. This high sensitivity is one reason for the poor coincidence between measured and computed translational modes, although the higher rotations are very well represented.

6.3 Response Analysis of Hybrid Structure

The strategy of the response computation for the hybrid structure is similar to the simulation when the engine is fixed to ground. Again, three phases are considered: static equilibrium, acceleration of crankdrive and stationary state. However, this is not a straight forward procedure which guarantees convergence of the numerical integration. It has to be noted that the structure represents a nonstationary, nonlinear dynamic problem with 15000 DOF’s which involves large rigid body motions and spatially variable excitation forces. Any solution algorithm has only a certain window of parameter settings which enables convergence. For example, a reduction of the time step length does not necessarily lead to better convergence conditions of the numerical integration. The convergence is also sensitive to modeling details, like e.g. axial rotational restraints of the pistons, statically overdetermined support of shafts, etc. [16]. The most critical numerical phase is the start of the crankdrive revolutions. Once a set of appropriate integration parameters is adjusted, the solution is rather fast. The computation time for 40 crankshaft revolutions was about 2 hours on a SGI Octane workstation.

The response was computed for a series of engine speeds at idle gear. For each revolution speed, the time series and frequency transform of the steering wheel vibrations and the engine mount forces were analyzed. Figure 9 shows an example of engine mount forces. The diagram corresponds to the case of “engine fixed to ground”, depicted in figure 6. Although the time series appear to be rather similar, the frequency transforms show significant differences.

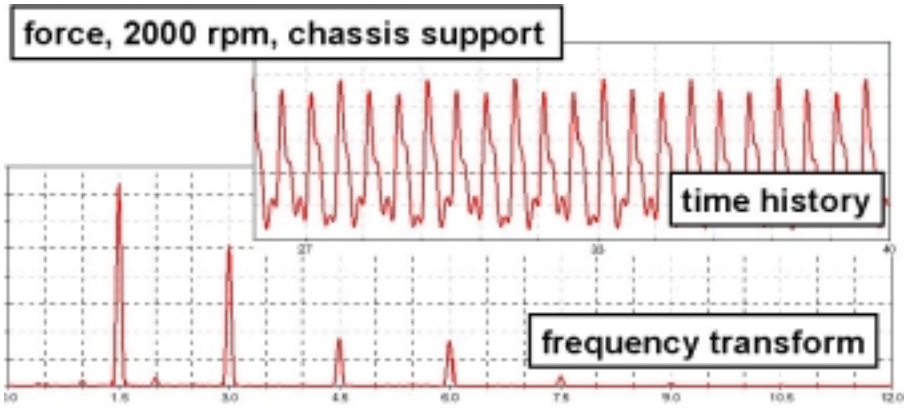

Figure 9: Forces in engine mount, 2000 rpm, support by chassis.

The response of different engine speeds can be summarized in form of a waterfall diagram (figure 10). This type of chart is well established in measurement data processing. The horizontal axes is the engine speed, the vertical axis represents the frequency. Moving from low to high engine speeds can be considered as a slow speed-up run under idle load. The size of the bulbs represents the magnitude of the response. Major response contributions occur at the frequencies of half or full engine orders. This results in straight traces of bulbs, where each trace represents an excitation order. A larger inclination means a higher engine order.

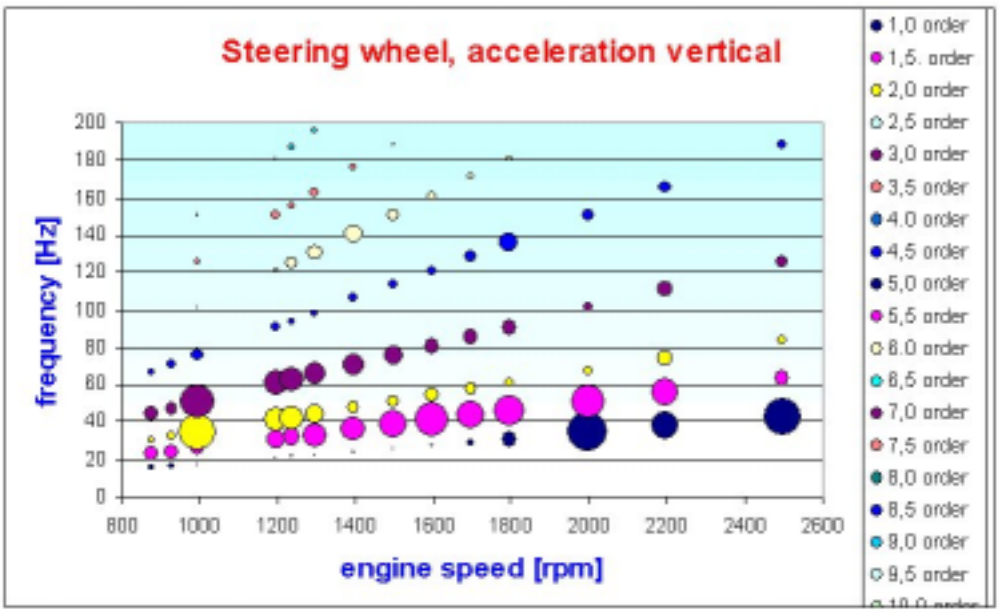

Figure 10: Computed response at steering wheel, waterfall chart, 800 - 2500 rpm.

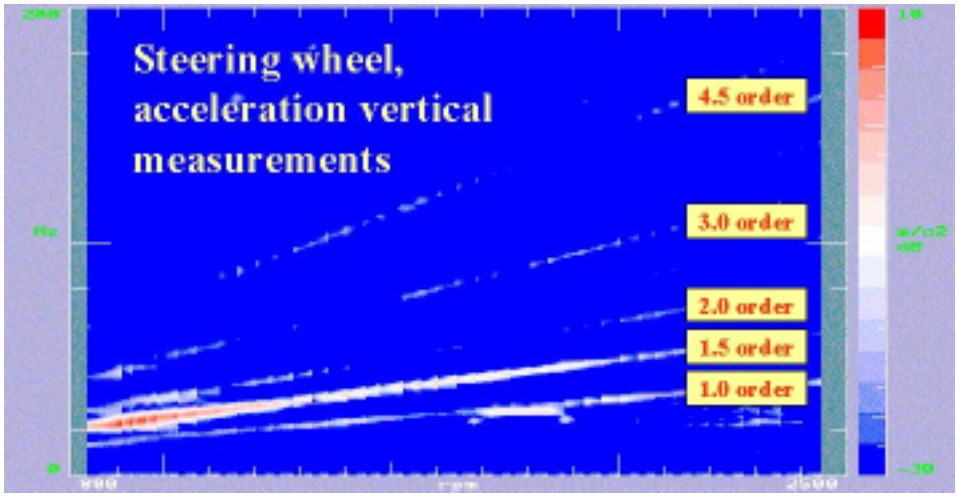

Figure 11: Measured response at steering wheel, waterfall chart, 800 - 2500 rpm.

Figures 10 and 11 are the comparison of computed and measured results of the steering wheel vibrations for the same range of engine speeds and frequencies.

- *The 1.0 engine order* is the lowest visible trace. The simulation and the measurements show relative small response contributions up to 1700 rpm. Around 1800 rpm, the first order starts to excite the steering wheel modes.Computed and measured response increase.
- *The 1.5 engine order* is the next trace. It is the dominating excitation order of the three cylinder engine. Measurements and simulation show this dominance over the entire range of speeds. However, the simulation underestimates its relative contribution up to 1500 rpm.
- *The 2.0 order* has its main contributions between 800 and 1400 rpm. It vanishes almost around 1800 rpm and increases again slightly for speeds higher than 2000 rpm.
- *The 2.5 order* does not appear in simulation and measurements.
- *The 3.0 order* has its main contribution around 1000 rpm. A slight trace appears for speeds around 2000 rpm.
- *The 3.5 and 4.0 orders* show no response in both charts.
- *The 4.5 order trace* is again visible. It has main contributions between 1100 and 1800 rpm.

7 STRUCTURAL IMPROVEMENTS

7.1 Stiffening of Chassis, Removing of Engine Mount

Supported by the simulation results, precise structural improvements could be realized. One major modification was the reduction of the number of engine supports

from four to three. One engine mount was simply removed. This mount carried only a small static load but had a low vibration impedance, i.e. it contributed significantly to the chassis vibrations.

Another major modification was the stiffening of the vehicle front girders by a transverse bar. This improved the sensitive interaction between the lowest engine translation modes and deformations of the vehicle front end. Additionally, the eigenfrequencies of the steering wheel were increased by a stiffer integration of the front plate which supports the steering column.

7.2 Validation of Improvements

The modifications resulted in significant improvements of the vibration and noise level of the vehicle. The annoying steering wheel vibrations were practically removed. The average interior noise level at idle gear was reduced by about 4 dB.

The improvements of exterior noise are shown in figure 12. The upper chart depicts the results of the standardized ISO R 362 test, where a vehicle passes under acceleration at a distance of 7 m. The adapted vehicle with the 3 cylinder diesel engine is 3 dB better than the original 4 cylinder diesel engine. Similar improvements were obtained for the exterior noise at idle gear for engine speeds between 800 and 2500 rpm. The lower chart of figure 12 compares the integral level of a series of microphone positions at 7 m distance around the car. The M13 application is better over the entire frequency range. The largest improvements are observed at higher engine speeds.

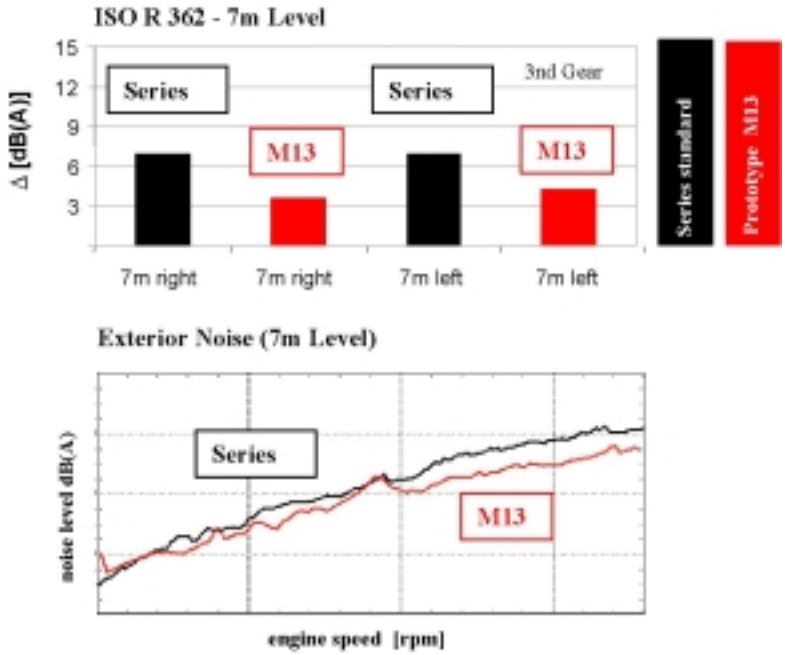

Figure 12: Comparison: series vehicle with 4 cylinder engine - adapted vehicle with 3 cylinder engine.

8 CONCLUSIONS

The Steyr 3 cylinder direct injection diesel engine (M13) was attached into the Fiat Brava Chassis. Extensive numerical simulations were performed to understand and optimize the complex vibration behaviour and the engine – chassis interactions.

The computation model was a hybrid structure of the FE chassis and a Multi Body model of the engine. The hybrid model includes the nonlinearities of the engine mounts and the internal excitation mechanisms of the engine. The FE part is rather coarse, so it has to be tuned to represent a specified set of modes. The total structure was assembled by component mode synthesis within the MBS software. Time histories of engine mount forces and of accelerations at the steering wheel (typical comfort location) are computed. The results are summarized in waterfall charts and compared to measurements of engine speed-up runs.

The simulations show a strong interaction of engine and chassis at the lowest modes. The analysis of the isolated systems “engine fixed to ground” and “chassis without engine” provide valuable information of basic structural properties but cannot predict the vibrations of the assembled system.

ACKNOWLEDGEMENTS

This project was partially supported by the Austrian Industrial Research Promotion Fund (FFF) under contract No. 3/12370, which is gratefully acknowledged. Thanks are due to Prof. H. Jericha, Technical University of Graz, Austria, and the ADAMS technical support, Germany, for their help and discussions.

REFERENCES

1. Ebersberger, I., Riepl, A., Kern, G., Knott, H.-P., *Schwingungssimulation eines allradgetriebenen Fahrzeugs*, ATZ Automobiltechnische Zeitschrift, Vol. 11, 1998, pp. 828-830.
2. Powell, N. N., March, J. P., *Practical Applications of Dynamic System Modelling in Powertrain and Vehicle Refinement*, 1st International Symposium on Multi-body Dynamics: Monitoring and Simulation Techniques, University of Bradford, U.K., 25-27 March 1997, pp. 47-57.
3. Eichlseder, W., Dannbauer, H., *Unter-suchung des akustischen Verhaltens einer Traktorkabine mit der Finite Elemente Methode*, XXIII International FEM-Congress, 1994, Baden-Baden, Deutschland.

4 Mühlmeier, M., Eckert, D., *Methode zur akustischen Analyse von Fahrzeug-karosserien und deren Auslegung*, VDI Berichte Nr. 1285, 1996, pp. 161-179.

5. Wartha, J., Dornauf, E., Schilling, W., *Ermittlung geeigneter Strukturmaß-nahmen zur Reduzierung des Innen-raumgeräusches von Kraftfahrzeugen*, VDI Berichte Nr. 1007, 1992, pp. 419-431.

6. Mitschke, M., Klingner, B., *Schwingungs-komfort im Kraftfahrzeug*, ATZ Automobiltechnische Zeitschrift, Vol. 1, 1998, pp. 18-24.

7. SYNGE J. L., BYRON A.G., 1959, *Principles of Mechanics*, McGraw Hill Book Company, p. 436, Equation 15404 and 15405

8. CRAIG, R. R, BAMPTON M. C. C., 1968, *Coupling of Substructures for Dynamics Analysis*, AIAA Journal, vol. 6, pp. 1313-1319

9. ADAMS/FEA Reference Manual Version 8.0; MDI - Mechanical Dynamics Incorporated, Ann Arbor, Michigan, U.S.A., 1998, page 15 - 19

10. Oyadiji, S. O., Choi, S. R., *Predicting the dynamic characteristics of sandwich rubber mounts using FEA*, Proceedings of ISMA23 - 1998 International Conference on Noise and Vibration Engineering, Katholieke Universiteit Leuven, Belgium, ed. P. Sas, Vol. 2, pp. 1055-1062.

11. Argyris, J., Mlejnek, H.-P., *Dynamics of Structures*, North - Holland, Amsterdam, 1991, ISBN 0-444-89045-9.

12. Craig, R. R., *Structural Dynamics - An Introduction to Computer Methods*, John Wiley & Sons, New York, 1981, ISBN 0-471-04499-7.

13. Craig, R. R., Bampton, M. C. C., *Coupling of Substructures for Dynamic Analysis*, AIAA Journal, 1968, Vol. 6, pp. 1313-1319.

14. Ottarson, G., *Modal Flexibility Implementation in ADAMS/FEA*, MDI -Mechanical Dynamics Incorporated publication, Ann Arbor, Michigan, U.S.A., 1997.

15. ADAMS/FEA Reference Manual Version 8.0, MDI - Mechanical Dynamics Incorporated, Ann Arbor, Michigan, U.S.A., 1998.

16. Witteveen, W., *Elastic Multi Body Simulation of the Crankdrive with Nonlinear Oil Film Structure Interaction,* Diploma Thesis, Johannes Kepler University Linz, Austria, 1999.